Characterizing Bubble Size Distribution and Generation Position in Iron Oxide-Containing Slag Smelting Reduction

K. Ohno[1] *and T. Kon*[2]

1. Professor PhD, Kyushu University, Fukuoka Fukuoka 819-0395. Email: ohno.ko-ichiro.084@m.kyushu-u.ac.jp
2. Assistant professor PhD, Kyushu University, Fukuoka Fukuoka 819-0395. Email: ohno.ko-ichiro.084@m.kyushu-u.ac.jp

Keywords: slag foaming; bubble formation; Iron oxide slag; smelting reduction; high-resolution X-ray CT

ABSTRACT

Slag foaming is an important control item in the process of refining molten steel. This study aims to investigate the factors controlling slag foaming by observing the bubble formation behaviour resulting from the chemical reaction between iron oxide and Fe-C alloy in the slag. In this study, 0.06 g of Fe-C alloy was introduced at the bottom of a BN crucible, and 6.0 g of slag (SiO_2:CaO:Fe_2O_3 = 40:40:30) was placed on top of it. The crucible was positioned inside an infrared image heating furnace, where the temperature was rapidly raised to 1370°C at a rate of 1000°C/min in a nitrogen stream, and then held at that temperature for a predetermined time before rapid cooling. Following rapid cooling, the internal structure of the sample was examined using a high-resolution X-ray CT device. The spherical equivalent volume was calculated based on the number of observed bubbles and their equivalent circle diameter. Additionally, the relationship between the volume ratio of small bubbles in the slag volume and the distance from the bottom of the crucible was determined, along with the calculation of bubble density and volume ratio. Under various experimental conditions, numerous bubbles with equivalent circular diameters ranging from 200 to 300 μm were consistently observed. The density and volume fraction of bubbles with circular equivalent diameters between 200 and 500 μm showed a tendency to increase as the distance from the bottom of the crucible increased. Bubbles with equivalent circular diameters of 500 μm or more consistently exhibited lower bubble densities, regardless of their height within the crucible. The formation of larger bubbles is attributed to a decrease in iron oxide concentration within the slag as the reaction progresses. However, this is believed to be due to their higher buoyancy, resulting in shorter residence times within the slag and a reduction in the number of encapsulated bubbles.

INTRODUCTION

Research into the steel refining process has delved into the effective utilization and control of slag. Particularly, with the advent of the oxygen steelmaking process, steel production has grappled with challenges arising from the dispersion of slag and molten iron induced by slag foaming. Slag foaming, a phenomenon wherein gas is introduced into low-basicity slag, resulting in gas retention and a substantial increase in slag volume, has been identified as a significant concern. Notably, managing slag foaming in recycling processes involving the melting and reduction of slag using electric furnaces has emerged as a critical issue (Harada, Hirata, Arai *et al*., 2018a, 2018b; Nakase, Matsui, Nakai *et al*., 2021). The judicious selection of the carbon source (Harada, Hirata, Arai *et al*., 2018a, 2018b) plays a crucial role in regulating foaming behavior. Addressing this challenge is integral to ongoing efforts in new iron source manufacturing processes, such as those integrating fluidized bed reduction and smelters like COREX. Additionally, research has highlighted the significance of employing estimation models based on machine learning to control the height of slag foaming (Son, Lee, Hwang *et al*., 2021). The optimization of these processes is pivotal in addressing current challenges and advancing the field of steelmaking.

The occurrence of slag foaming in molten slag during steel refining processes is a prevalent phenomenon in various refining procedures utilizing top-blown oxygen, such as converters, hot metal pre-treatment, smelting reduction, and scrap melting with the use of fossil fuels (Hara and Ogino, 1992; Nakase, Matsui, Nakai *et al*, 2021). Specifically, during the dephosphorization treatment conducted in hot metal pre-treatment, silicon within the hot metal undergoes desiliconization before the dephosphorization reaction, resulting in the formation of slag with low basicity. In situations where dephosphorization treatment is executed in the presence of such low basicity slag, slag foaming occurs due to the CO gas generated by the concurrent decarburization reaction and the carrier gas used to inject the dephosphorization agent. Containers employed in the hot metal pre-treatment process, such as torpedo cars and ladles, possess smaller freeboards compared to converters. Consequently, in the event of slag foaming, there is a risk of slag overflow from the container. This has a substantial impact on productivity and workability, as it necessitates time-consuming efforts to restore the lower part of the furnace (Mukai, 1991; Harada, Hirata, Arai *et al*, 2018a). Moreover, the iron, intended as the final product, becomes emulsified within the slag, leading to a reduction in the yield of iron.

Due to these challenges, the phenomenon of slag foaming has garnered significant attention and research efforts since the early stages of Basic Oxygen Furnace (BOF) steelmaking technology. When delving into the mechanism of slag foaming, it becomes imperative to categorize influencing

factors, distinguishing those related to the generation process—such as the velocity of gas production resulting from reactions and the dimensions of bubbles—and those regulating the stability of the generated bubbles. To scrutinize the stabilizing factors associated with bubbles, various approaches are conceivable. One approach involves measuring the elevation of the top surface of the slag by introducing gas into the molten metal at a constant flow rate. Alternatively, the cessation of gas injection post-foaming allows the top surface of the bubbles to ascend to a certain height due to bubble disruption.

In assessments utilizing cold models designed to simulate foaming slag at ambient temperature, endeavors have been made to modulate foam generation behavior through the incorporation of fine solid-phase powder and liquid-phase particles (Martinsson, Vickerfält, and Sichen, 2022). Moreover, studies involving measurements of liquid-phase viscosity, encompassing the gas phase (Hatano, Hayashi, Saito *et al*, 2021) have indicated the significance of controlling the interfacial energy between solid-gas and liquid phases. There have also been investigations into the size and growth patterns of bubbles within cold models, as these aspects are pivotal in managing foaming behavior and viscosity measurements (Zhang, Wang, Hu *et al*, 2021). It has been documented that bubbles ascending to the surface and persisting there tend to adopt non-spherical shapes.

In their study conducted at the elevated refining temperature, Cooper and Kitchener (1959) explored the slag-foaming characteristics of the CaO-SiO_2-P_2O_5 melt. The investigation revealed that binary CaO-SiO_2 melts do not exhibit foaming tendencies; however, the introduction of P_2O_5 to melts with more than 50% SiO_2 content induces pronounced foaming. It was observed that the longevity of bubbles increased proportionally with higher P_2O_5 and SiO_2 concentrations. Subsequent research by Hara, Ikuta, Kitamura et al. (1983) and Hara, Yunoki, and Ogino (1989) involved the measurement of bubble lifetime and height in CaO-SiO_2-FeO and Na_2O-SiO_2 melts through gas injection, establishing a significant correlation between bubble lifetime and surface tension. Studies have reported a substantial increase in bubble lifespan attributed to a reduction in surface tension. In a separate investigation, Ito and Fruehan (1989) derived the foaming index, representing the bubble lifetime, as a function of viscosity and surface tension in a FeO-CaO-SiO_2 melt. This experiment involved the introduction of Ar gas through a capillary tube. The foaming index proposed by Ito and Fruehan is presented below.

$$\Sigma = 570 \frac{\mu}{\rho\sigma} \quad \ldots(1)$$

Here, Σ is the life of the foam (s), μ is the viscosity of the slag (Pa s), ρ is the density of the slag (kg/m^3), and σ is the surface tension (N/m). The foaming index facilitates an explication of the observation that the longevity of a bubble increases proportionally with escalating viscosity and diminishing surface tension. Notably, the investigations conducted employed blowing nozzles featuring relatively large inner diameters of 2.1 mm and 2.5 mm, resulting in the formation of correspondingly sizable bubbles. This raises concerns regarding the fidelity of the reproduction of bubble characteristics in the actual process. Mukai (1991) posits that bubbles generated through gas injection via a capillary tube differ from those originating from gaseous products formed in a chemical reaction within the authentic industrial process. In the industrial scenario, slag foaming transpires as iron oxide within the slag, floating atop the hot metal, reacts with the carbon present in the hot metal at the vessel's bottom due to gravitational forces. Consequently, it becomes imperative to scrutinize bubbles generated through the chemical interaction between FeO and Fe-C alloy.

Moreover, predominant scholarly inquiries thus far have delved into the correlation between the physical attributes of slag and the stability of foam. These investigations have encompassed aspects such as the internal structure of foamed slag and the behavior of CO bubbles regarding their generation and distribution. In the 1980s, the methodology of direct observation employing transmitted X-rays was employed to scrutinize the slag bubbling phenomenon induced by gases resulting from reactions mirroring actual operational conditions. Notably, an examination of the interaction between slag melt containing iron oxide and carbon-saturated iron (Ogawa and Tokumitsu, 2001) has revealed a discernible relationship between the height of slag foaming and

alterations in bubble diameter. Specifically, heightened foaming was observed when small bubbles were generated, while a pronounced decrease in foaming occurred concomitantly with an increase in bubble diameter. This observation intimates that the progression involving the formation, coalescence, growth, and breakdown of microbubbles is integral to the lifespan of the bubbles. Additionally, scholars (Drain, Gu, Dogan et al, 2021) have underscored the significance of regulating slag viscosity in assessing decarburization and dephosphorization reactions induced by emulsions dispersed in the slag. Nevertheless, owing to limitations in X-ray transmission resolution, attaining proximity to the formation processes of microscopic bubbles measuring 1 mm or less proves challenging. Therefore, an imperative need exists to elucidate the intricate mechanisms governing the formation of microscopic bubbles.

Our investigation endeavors to examine slag foaming resulting from the chemical interaction between FeO and Fe-C alloy within slag, emphasizing physical attributes such as the size and distribution characteristics of CO bubbles comprising the foam. The primary objective of this study is to elucidate the mechanisms of slag foaming and identify the determinative factors governing slag foaming through an analysis of its internal structure. Specifically, our research centers on the dimensions and spatial arrangement of gas bubbles, with a novel emphasis on scrutinizing the generation and distribution patterns of microscopic air bubbles measuring 1 mm or smaller in diameter.

EXPERIMENTAL METHOD

In this investigation, aimed at simulating slag foaming during hot metal pre-treatment arising from the interaction between slag and pig iron, particular attention was directed towards the microbubbles produced through the reduction reaction involving iron oxide in the molten slag and carbon in the Fe-C alloy. The distribution patterns of bubbles within the evolving slag were scrutinized employing the methodology outlined below.

Experimental sample

The basic system of slag generated during hot metal pre-treatment is the CaO-SiO_2-Fe_xO ternary system. In this investigation, the principal constituents of the slag comprised CaO, SiO_2, and Fe_2O_3, with a selected CaO/SiO_2 basicity ratio of 1 for simplicity. In consideration of the challenges associated with handling iron oxide, stemming from variations in iron valence during slag preparation and experimental execution, this study opted for the utilization of Fe_2O_3 due to its straightforward nature. In order to observe bubbles smaller than 1 mm, this study adopted a Fe_2O_3 concentration of 40 mass%, which has a relatively lower viscosity, compared to lower iron oxide containing slag. Special grade reagents SiO_2, $CaCO_3$, (all reagents manufactured by Sigma-Aldrich Japan Co., Ltd., purity: ≥99.0) and Fe_2O_3 (99.8%-Fe, manufactured by Strem chemicals) were used in the experiment. Taking into account the thermal decomposition of $CaCO_3$, each sample was weighed to have a predetermined composition and thoroughly mixed using an Al_2O_3 mortar. The mixed powder was filled into a platinum crucible and melted in an air atmosphere at 1500°C for 1 hour. Thereafter, it was poured onto a copper plate and rapidly cooled, and the resulting glassy slag sample was pulverized to under 600 μm.

The carbon concentration of the iron-carbon alloy specimen employed in this investigation was 0.63 mass%. The aforementioned iron-carbon alloy specimen constituted a standardized sample (fabricated by the Japan Iron and Steel Federation) and its compositional details are delineated in Table 1. The iron specimens underwent preparation by grinding to achieve a particle size ranging from approximately 1 to 2 mm prior to utilization.

TABLE 1 – Chemical composition of Fe-C alloy (mass%)

C	Si	Mn	P	S	Cu	Al	N_2
0.63	0.24	0.48	0.0058	0.0027	0.008	0.03	0.0028

Experimental method

The objective of this experimental study was to investigate slag foaming, a critical issue in hot metal pre-treatment, with a focus on observing slag foaming at approximately 1400°C. To minimize the occurrence of reactions during temperature elevation and reduction processes and to observe the state in which slag foaming takes place, it was imperative to control reactions before slag foaming and rapidly cool the system while sustaining the slag foaming phenomenon. Consequently, an infrared image heating apparatus capable of swift heating and cooling was employed in this investigation.

The apparatus employed in this experiment comprised an infrared image heating furnace in the central stage, a furnace core tube, a lifting mechanism for the sample crucible in the lower stage, and a cooling chamber. The capability for rapid temperature rise and rapid cooling was achieved through the integration of an infrared image heating furnace, an elevating sample crucible, a cooling chamber, and an air-cooled quartz reaction tube known for its high resistance to thermal shock.

A R-type thermocouple, positioned inside the graphite rod as depicted in Fig. 1(a), was utilized for temperature measurement and control of the sample. Given that the height of the slag increases due to slag foaming, measures were taken to prevent direct contact between the slag and the graphite rod. To mitigate temperature differentials between the furnace interior and the thermocouple, the graphite rod was strategically positioned such that its lower end aligned with the upper end of the BN crucible, as illustrated in Fig. 1(b).

The sample crucible employed consisted of a graphite crucible (outer diameter 36 mm, inner diameter 30 mm, height 40 mm), while a BN crucible (outer diameter 25 mm, inner diameter 20 mm, height 32.5 mm) was utilized. As depicted in Fig. 1(c), Fe-C alloy and slag were sequentially charged into the BN crucible, with the weights adjusted to 0.06g for Fe-C alloy and 6.0g for slag. Following the sample charging, the crucible was placed in an infrared image heating furnace, where the temperature was rapidly elevated to 1370°C at a rate of 1000°C/min under an inert atmosphere with an N2 flow rate of 2NL/min. Subsequently, the sample was held at the set temperature for a predetermined duration and then swiftly cooled at 1000°C/min using a quenching chamber.

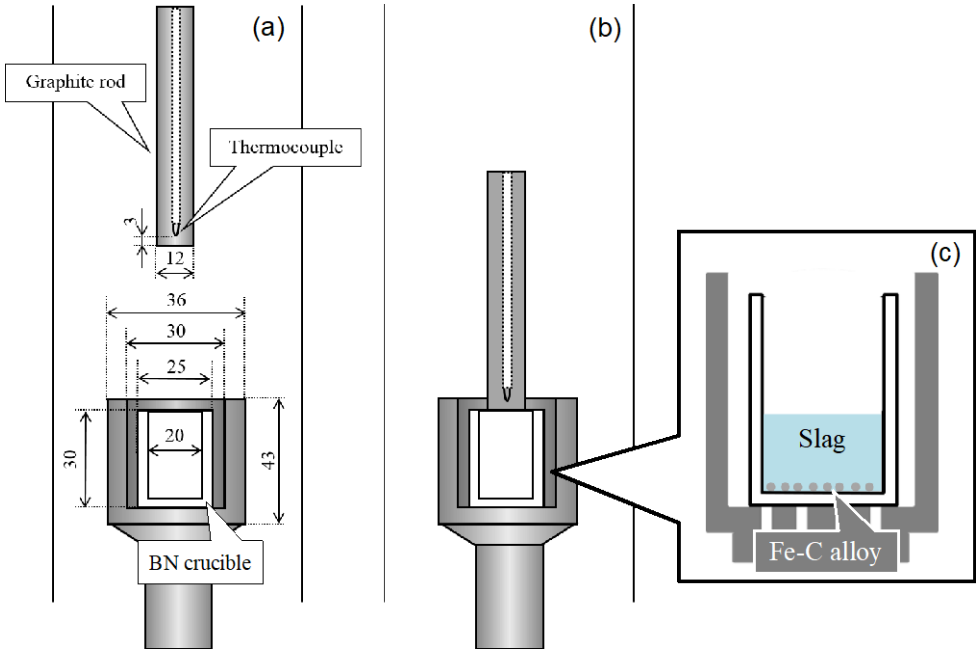

FIG 1 – Schematic illustration of sample holder part and sample setting.

3D X-ray CT imaging

In the present investigation, we employed a high-resolution three-dimensional X-ray computed tomography (CT) apparatus, specifically the SKYSCAN 1172 model manufactured by BRUKER, to scrutinize the spatial distribution of bubbles within the cross-sectional profile of the foaming slag. The CT equipment exploits variations in X-ray transmittance and absorption coefficient to capture detailed structural information. This is achieved by situating the specimen on a revolving pedestal

and subjecting it to X-ray irradiation during rotation. Consequently, regions of heightened X-ray absorption are discerned, allowing for the reconstruction of a tomographic cross-sectional view by compiling absorption data at specific positions on the object.

The experimental parameters were set as follows: Camera Pixel Size of 9.00 μm, Image Pixel Size of 20.00 μm, Source Voltage of 80 kV, Source Current of 100 μA, Exposure time of 2000 ms, and Rotation Step of 1.2 degrees. These conditions facilitated the acquisition of high-quality imaging data, enabling the accurate calculation of ratios and the subsequent construction of a detailed cross-sectional representation of the specimen.

RESULTS AND DISCUSSION

After conducting the experiment, a cross-sectional examination of each specimen was carried out utilizing a computed tomography (CT) apparatus. An exemplar depiction of the observation of a specimen rapidly cooled and held for 2 minutes is presented in Figure 2. Through CT imaging, both a horizontal cross-sectional perspective of the crucible (depicted in Fig. 2(a)) and a vertical cross-sectional view (illustrated in Fig. 2(b)) were acquired, enabling the discrimination of slag, iron, air bubbles, and voids. In the illustration, the grey region corresponds to slag, while the white masses represent iron. Additionally, the small black circular features within the slag indicate the presence of air bubbles, whereas the larger black regions signify voids.

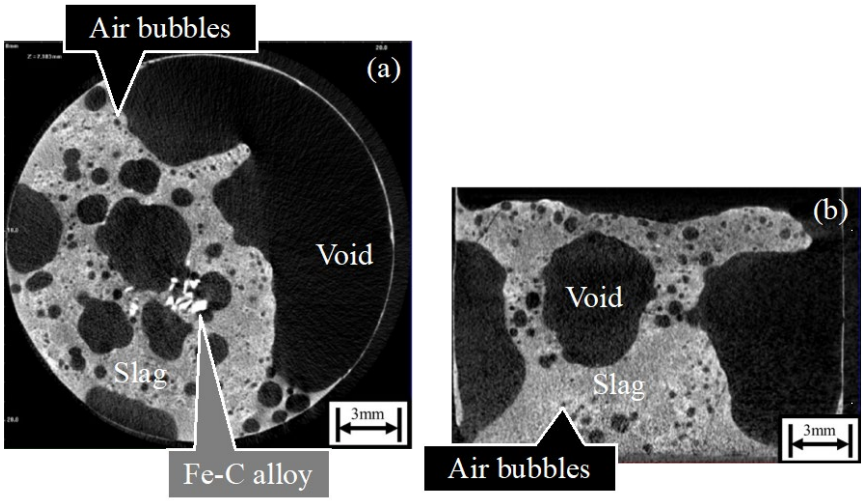

FIG 2 – Cross-sectioning photographs of quenched sample in BN crucible in (a) Radial section, and (b) Vertical section (Hold for 2.0 minutes).

Evaluation based on circle equivalent diameter distribution

The evaluation of slag foaming was conducted through the analysis of the distribution of equivalent circle diameters. The equivalent circle diameter distribution is defined as the distribution of diameters of circles corresponding to a specified area of a given cross section. Following the acquisition of cross-sectional images of the crucible using CT imaging, these images were colorized and organized based on the range of equivalent circle diameters. To ensure a comprehensive analysis of the entire crucible cross-sectional direction, the minimum equivalent circle diameter was set between 200 and 300 μm, accounting for the resolution and pixel count of the CT images obtainable. Additionally, areas in the crucible where the equivalent circle diameter range was not depicted were identified as slag. This methodology facilitated the organization of the size, number, and positional relationship of bubbles. Figure 3 presents a horizontal cross-sectional view of the crucible captured using a CT device after each experimental run. Given the scarcity of bubbles exceeding 2 mm in size, the crucible cross-section was observed at 2 mm intervals.

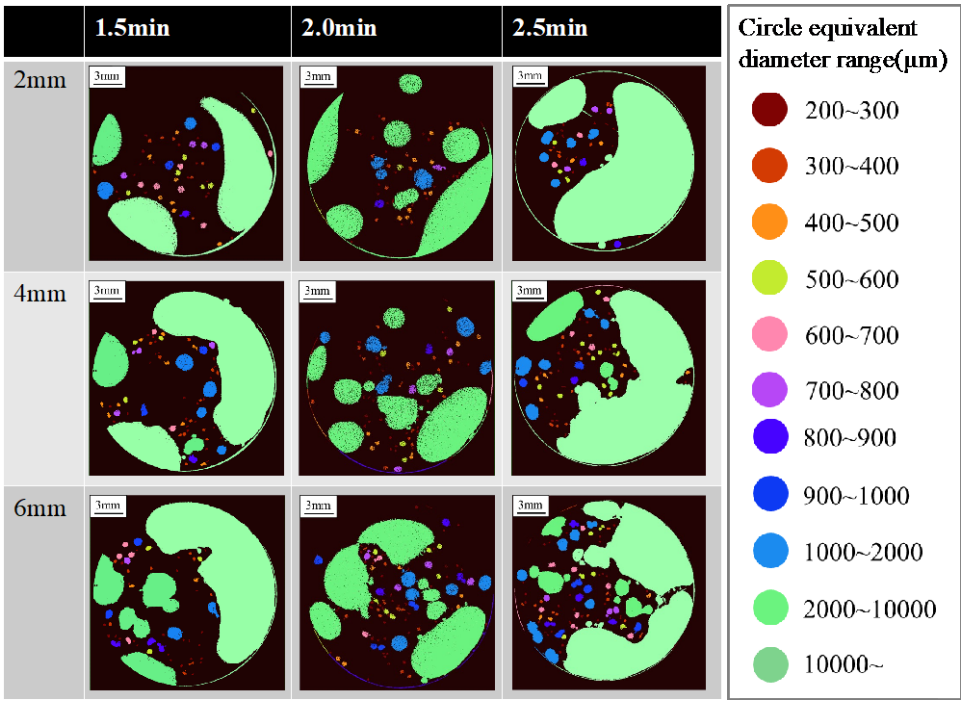

FIG 3 – Radial-sectional observation of quenched samples for each holding time and distance from the bottom of the crucible using micro-CT observation..

Three-dimensional evaluation of slag foaming

Three-dimensional evaluation is necessary to understand the internal structure of slag foaming in more detail. Therefore, as shown in Fig. 4, the foaming slag was carved into 1 mm height increments, and the volume of air bubbles and cavities present in a 1 mm height cylinder was calculated and analysed from a two-dimensional cross-sectional view.

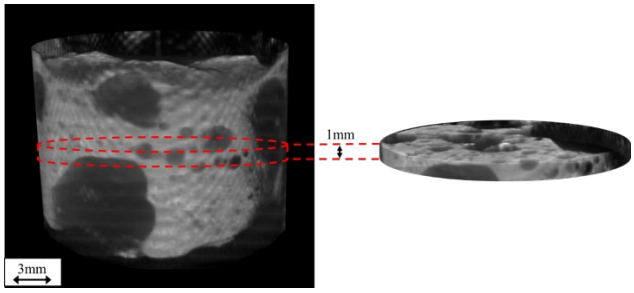

FIG 4 – 3D image of foaming slag and 3D evaluation method (Hold for 2min).

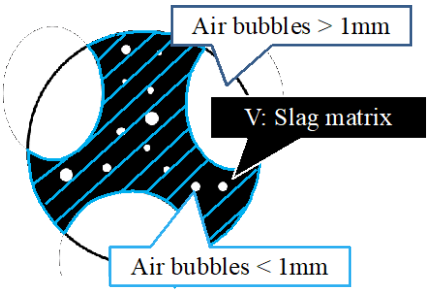

FIG 5 – Schematic illustration of small air bubbles evaluation method.

The primary objective of this investigation was to assess the distribution characteristics of air bubbles within the slag. Consequently, the substantial voids evident in each cross-sectional analysis were omitted, and emphasis was placed on the evaluation of minute air bubbles embedded within the slag. Denoting the volume of a cylinder with a 1 mm thickness, excluding portions exhibiting an equivalent circular diameter of 1 mm or greater as V (mm^3), and representing the number of small

bubbles within each cross section as n (-), the bubble density N (/mm^3) was articulated in the ensuing manner.

$$N = n/V \quad (/mm^3) \quad \cdots(2)$$

Figure 6 illustrates the correlation between bubble density and the distance from the bottom of the crucible for various bubble sizes. The data depicted in this figure indicates that a decrease in the equivalent circular diameter of bubbles is associated with an increase in bubble density. This observation suggests that smaller bubbles exhibit a lengthened residence time, while larger bubbles swiftly ascend and exit the slag due to the fact that, under uniform viscosity conditions, smaller bubbles have a lower terminal velocity. Across all experimental parameters, the bubble density of bubbles with an equivalent circular diameter ranging from 200 to 500 μm rises proportionally with the distance from the bottom of the crucible. Additionally, the bubble density of bubbles with an equivalent circular diameter of 500 to 1000 μm demonstrates an increasing trend independent of the height. Notably, a discernible tendency of density reduction becomes evident.

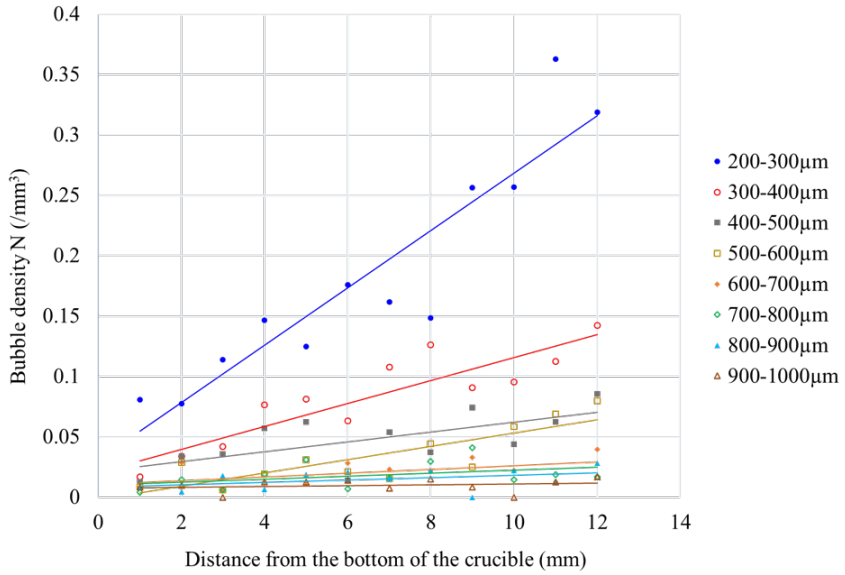

FIG 6 – Relationship between the distance from the bottom of the crucible and the bubble density for each bubble size (Hold for 2.0 min).

Mechanism of bubble generation and distribution

Utilizing the acquired results, Figure 7 illustrates a schematic depicting the progression of bubble generation and distribution.

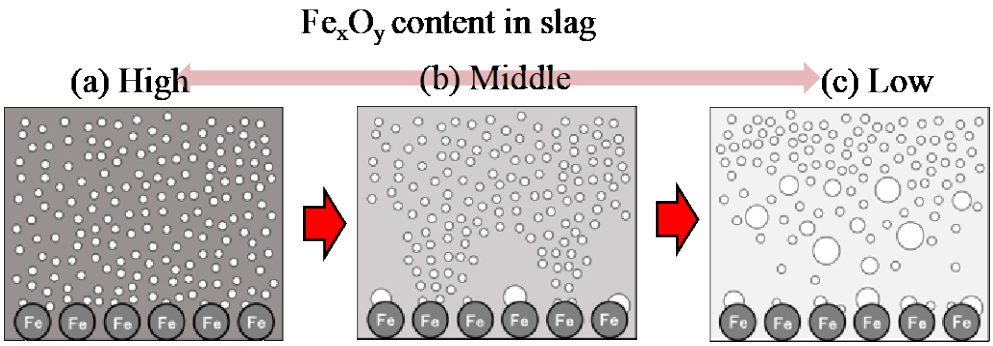

FIG 7 – Relationship between the distance from the bottom of the crucible and the bubble density for each bubble size (Hold for 2.0 min).

Upon initiation of the reaction, diminutive bubbles manifest, as depicted in Fig. 7 (a), leading to an elevation in the liquid level. The diminishing iron oxide concentration within the slag during the progression of the reaction is postulated. Notably, Ogawa and Tokumitsu (2001) conducted a study revealing an augmentation in the size of bubbles at the slag/metal interface as the iron oxide concentration diminishes. Terashima, Nakamura, Mukai et al. (1992) proposed that the size of generated bubbles is contingent upon wettability. Moreover, Mukai, Furukawa, and Tsuchikawa (1977) quantified the contact angle between slag and molten iron, asserting an enhanced wettability with higher iron oxide concentration in the slag. Collectively, these reports suggest that as the iron oxide concentration diminishes, impeding the wetting of slag on molten iron, the bubbles burgeon in size. Conversely, when the iron oxide concentration is high, facilitating slag wetting on molten iron, the bubbles persist in a smaller size, forming at the interface. It is conceivable that these bubbles disengage from the interface and ascend to the surface. Consequently, as the iron oxide concentration wanes over time, larger bubbles may commence forming at the slag/metal interface, as illustrated in Fig. 7 (b). As small bubbles are not generated at the slag/metal interface where large bubbles are prevalent, it is inferred that the quantity of small bubbles generated diminishes compared to the initial stages of the reaction. Moreover, it is hypothesized that the bubble density of small bubbles, characterized by an equivalent circle diameter of 200 to 500 μm, decreases with an increasing distance from the bottom of the crucible. Additionally, with the progression of the reaction from the state depicted in Fig. 7 (b), the number of large bubbles generated intensifies, as evidenced in Fig. 7 (c). However, owing to their rapid ascent, the temporal residency of large bubbles within the slag is abbreviated, resulting in a presumed reduction in the number of entrapped bubbles. Consequently, it is posited that the bubble density remains low irrespective of the height, emphasizing the transitory nature of large bubbles within the system.

CONCLUSIONS

In this investigation, simulated slag composed of CaO, SiO_2, and Fe_2O_3 was utilized, and the dimensions and distribution of bubbles resulting from the chemical interaction between iron oxide and Fe-C alloy in molten slag at 1370°C were assessed employing an infrared image heating apparatus. The subsequent observations were made by examining the cross-section of the specimen post-quenching. Irrespective of the experimental parameters, numerous bubbles with equivalent circular diameters ranging from 200 to 300 μm were consistently observed. This phenomenon can be attributed to the principle outlined in Stokes' equation, indicating that, under constant slag viscosity, smaller bubbles exhibit lower terminal velocities and consequently longer residence times. The density and volume fraction of bubbles with circular equivalent diameters within the range of 200 to 500 μm exhibited an upward trend as the distance from the crucible bottom increased. This behavior is conjectured to stem from the temporal evolution wherein larger bubbles are progressively formed, leading to a reduction in the simultaneous generation of smaller bubbles. Bubbles with equivalent circular diameters exceeding 500 μm tended to manifest smaller bubble densities independent of their vertical position. The emergence of larger bubbles is attributed to the diminishing concentration of iron oxide in the slag as the chemical reaction advances, resulting in a heightened buoyant speed that curtails residence time in the slag and diminishes the count of bubbles.

ACKNOWLEDGEMENTS

The authors would like to express their gratitude to the research group “Slag Visualization Study Group for Understanding the Flow of Multiphase Melts” established at the Japan Iron and Steel Institute for financial support and scientific advice.

REFERENCES

C. F. Cooper and J. A. Kitchener, 1959. The foaming of molten silicates, *J. Iron Steel Inst.,* 193: 48-55

P. B. Drain, K. Gu, N. Dogan, R. J. Longbottom, M. W. Chapman, B. J. Monaghan, K. S. Coley, 2021. Dephosphorization Kinetics of Bloated Metal Droplets Reacting with Basic Slag Containing TiO_2, *ISIJ-Int.*, 61(3), 734-744

S. Hara, M. Ikuta, M. Kitamura and K. Ogino, 1983. Foaming of Molten Slags Containing Iron Oxide, *Tetsu-to-Hagané*, 69(9), 1152-1159 (in Japanese).

S. Hara, T. Yunoki and K. Ogino, 1989. Effect of Surface Viscosity on the Foaminess of Molten Oxides, *Tetsu-to-Hagané*, 75(12), 2182-2187 (in Japanese).

S. Hara and K. Ogino, 1992. Slag-Foaming Phenomena and the Suppression, *Tetsu-to-Hagané*, 78(2): 200-208 (in Japanese).

T. Harada, H. Hirata, T. Arai, T. Toh, T. Yamada, 2018a. Development of the Molten Slag Reduction Process -1 Characteristics of Closed Type DC arc Furnace for Molten Slag Reduction, *ISIJ-Int.*, 58(10):1934-1942

T. Harada, H. Hirata, T. Arai, T. Toh, C. Shuto, 2018b. Development of the Molten Slag Reduction Process -2 Optimization of Slag Reduction Process with Molten Slag Charging, *ISIJ-Int.*, 58(10): 1943-1952

S. Hatano, S. Hayashi, N. Saito, and K. Nakashima, 2021. Viscosity Evaluation of Simulated Foaming Slag via Interfacial Reaction at Room Temperature, *ISIJ-Int.*, 61(12): 2904-2914

K. Ito and R. J. Fruehan, 1989. Study on the foaming of CaO-SiO_2-FeO slags: Part I. Foaming parameters and experimental results, *Metall. Trans. B*, 20B: 509-514

J. Martinsson, A. Vickerfält, and D. Sichen, 2022. Impact of Solid Particles and Liquid Droplets on Foams – Cold Model and High Temperature Experiments, *ISIJ-Int.*, 62(1): 104-111

K. Mukai, H. Furukawa and T. Tsuchikawa, 1977. Effect of Iron Oxide in CaO-SiO_2, Slag on Interfacial Tension between Liquid Dilute Fe-Si-O Alloys and the Slag, *Tetsu-to-Hagané*, 63(9), 1484-1493

K. Mukai, 1991. Some Views on the Slag Foaming in Iron and Steelmaking Processes, *Tetsu-to-Hagané*, 77(6): 856-858 (in Japanese).

K. Nakase, A. Matsui, Y. Nakai, N. Kikuchi, Y. Kishimoto, and I. Tetsuyama, 2021. Development of Iron Recovery Technique from Steelmaking Slag by Reduction at High Temperature, *Tetsu-to-Hagané*, 107(9):693-700 (in Japanese)

Y. Ogawa and N. Tokumitsu, 2001. X-ray Fluoroscopic Observation of Slag Foaming, *Tetsu-to-Hagané*, 87(1): 14-20 (in Japanese).

K. Son, J. Lee, H. Hwang, W. Jeon, H. Yang, I. Sohn, Y. Kim, and H. Um, 2021. Slag foaming estimation in the electric arc furnace using machine learning based long short-term memory networks, *J. Mater. Res. Tech.*, 12: 555-568

H. Terashima, T. Nakamura, K. Mukai and T. Odawara, 1992. The Foaming Mechanism of Iron-Silicate Slag, *Shigen-to-Sozai*, 108(10): 737-742

C. Yin, S. Zhang, Y. GuO, L. Wen, and C. Bai, 2022. Effect of Top Gas Recycling Technology on the Softening, Melting and Dropping Behavior of V–Ti Bearing Burden in COREX Process, *ISIJ-Int.*, 62(9): 1777-1784

B. Zhang, R. Wang, C. Hu, C. Liu, and M. Jiang, 2021. Effect of Viscosity on Dynamic Evolution of Metallurgy Slag Foaming, *ISIJ-Int.*, 61(5), 1348-1356